Author version: J. Geophys. Res. (B: Solid Earth), vol.116(5); 2011; 17 pp;
doi:10.1029/2010JB007800

Hotspot activity and tectonic settings near Amsterdam-St Paul plateau (Indian Ocean)

Janin, M.[1,2]*, Hémond, C.[1,2], Guillou, H.[3], Maia, M.[1,2], Johnson, K. T. M.[4], Bollinger, C.[1,2], Liorzou, C.[1.2], Mudholkar, A.[5]

(1) Université Européenne de Bretagne, 6 avenue Le Gorgeu, 29200 Brest, France.

(2) Université de Brest, CNRS Domaines Océaniques, Institut Universitaire Européen de la Mer, Place Copernic, 29280 Plouzané, France.

(3) LSCE/IPSL, Laboratoire CEA-CNRS-UVSQ Domaine du CNRS bât 12, Avenue de la Terrasse, 91198 Gif sur Yvette, France.

(4) School of Ocean and Earth Science and Technology, University of Hawaii, Honolulu, Hawaii 96822, USA

(5) National Institute of Oceanography, Dona Paula, Goa, 403004, India.

* Corresponding author: Myriam.Janin@univ-brest.fr

Keywords: ridge-hotspot interaction, K-Ar geochronology, SEIR, hotspot, Indian Ocean, Capricorn plate

Index terms: 1033 Intra-plate processes (3614, 8415), 1100 Geochronology, 3038 Oceanic plateaus and microcontinents, 8150 Plate boundary: general (3040), 9340 Indian Ocean.

Abstract:

The Amsterdam-St. Paul (ASP) plateau is located in the central part of the Indian Ocean and results from the interaction between the ASP hotspot and the South-East Indian Ridge (SEIR). It is located near the diffuse boundary between the Capricorn and Australian plates [Royer&Gordon, 1997]. The seamount chain of the Dead Poets (CDP) is northeast of the ASP plateau and may represent older volcanism related to the ASP hotspot; this chain consists of two groups of seamounts: (1) large flat-topped seamounts formed 8-10 Ma, and (2) smaller conical seamounts formed during the last 2 Myr. The ASP hotspot has produced two pulses of magmatism [Maia et al., this issue] that have been ponded under the ASP plateau and erupted along the divergent boundary between the Capricorn and Australian plates. The N65° orientation of the CDP, as well as the seamount's elongated shapes, support an opening motion between the Capricorn and Australian plates along a suture oriented in the N155° direction. This motion compared to the Antarctic plate amounts to an apparent velocity of 7.7 cm/yr northeastwards for the Capricorn-Australian block. This motion does not fit with a fixed plume model. We suggest therefore that the ASP plume experienced a motion of about 1-2 cm/yr to the SW, which is opposite to the asthenospheric flow in this region and suggests a deep-seated plume.

Author version: J. Geophys. Res. (B: Solid Earth), vol.116(5); 2011; 17 pp;
doi:10.1029/2010JB007800

Introduction

Interaction between ridges and hotspots occur in all oceans and in various geodynamic contexts. When a ridge is located directly above a plume the excess heat results in enhanced melting and magma production [Schilling, 1973; Vogt, 1976]. One of the main consequences is the construction of large oceanic plateaus, such as the Icelandic and Azores plateaus [Schilling et al., 1991; Gente et al., 2003]. In the Indian Ocean, the South-East Indian ridge (SEIR) has interacted with two hotspots over the last 40 Myr, which resulted in the construction of two oceanic plateaus: (1) the northern Kerguelen plateau, which started to form about 40 My ago [Frey et al., 2000] and (2) the Amsterdam-St Paul plateau, which has been active over the last 10 My [Maia et al., 2008].

The construction of these oceanic plateaus has been complicated by the fact that the history of plate motion in the Indian Ocean is complex. Three main diverging plates induced the formation of three spreading ridges: the Central Indian Ridge (CIR hereafter) between the African and Indo-Australian plates, the Southwest Indian Ridge (SWIR) between the African and Antarctic plates, and the Southeast Indian Ridge (SEIR) between the Indo-Australian and Antarctic plates. However, the plate motion in the Indian Ocean is inconsistent with a rigid Indo-Australian plate model [Minster et al., 1978, Stein et al., 1984; DeMets et al., 1988] and more likely is the result of the interaction between four distinct subplates (Indian, Capricorn, Australian and Macquarie) separated by diffuse boundaries [Minster&Jordan 1978; Wiens et al., 1985; DeMets et al., 1988; Royer&Gordon, 1997] (Fig 1). The Capricorn and Australian plates are divergent near the CIR and SEIR and their diffuse boundary seems to accommodate the resulting deformations. The actual boundary between the Capricorn and Australian plates intersects the SEIR near the St. Paul fracture zone (SPFZ) [Conder& Forsyth., 2001].

The Amsterdam-St Paul (ASP)/SEIR interaction system successively underwent the three possible geometries for the interaction of a ridge and a hotspot, that is to say the ridge approaches, overlies, and finally moves away from the plume. This makes it of special interest for the study of ridge-hotspot interactions. In addition, the proximity of Capricorn/Australian plate boundary may also have influenced the local volcanism and the construction of the plateau. This area was the target of the MD157/PLURIEL cruise (N/O Marion Dufresne, September/October 2006). This cruise was dedicated to map and sample the ASP plateau and the Chain of the "Dead Poets" (CDP) (fig. 2). Preliminary geophysical results obtained during the cruise have been presented elsewhere [Maia et al. 2008] and a detailed analysis of the surface magnetism, the gravity and the bathymetry is presented in two companion papers [Courreges et al., submitted; Maia et al., this issue]. This work presents a geochronological reconstruction of the volcanic features related to ASP hotspot prior and during its interaction with the SEIR.

I. Geological setting

1. Context of the study

The ASP plateau is a complex structure and the result of several processes. It is limited by the Amsterdam fracture zone (AFZ) toward the northwest, the St Paul fracture zone (SPFZ) toward the southeast and is crosscut by the SEIR (fig. 2). This plateau is mostly submarine with only two subaerial features, the Amsterdam and St Paul islands. They are located 80km apart and are younger than 0.4 Ma [Watkins et al., 1975]. Their isotope compositions clearly indicate that they derive from a mantle plume distinct from the Kerguelen hotspot [Doucet et al., 2004]. Recently, the Boomerang expedition Leg 9, on the SEIR between 77 and 88°E (R/V Melville, 1996), discovered a small active seamount on the ASP plateau, near the SEIR Segment I (following the names of Royer&Schlich, 1988)

[Johnson et al., 2000]. This cruise collected dredge samples and published a complete geochemical study of SEIR Segments I and J that currently are crossing the ASP plateau [Nicolaysen et al., 2007]. This work suggests a heterogeneous source at a rather small scale, but their limited geographical coverage does not allow a representative picture of the whole geodynamic evolution of the ASP plateau to be developed.

The ASP plume, presently located beneath Amsterdam and St Paul islands, was originally located beneath the Australian Plate. The interaction phase with the SEIR and the construction of the ASP plateau began about 10 Ma ago [Maia et al., 2008]. Observed magnetic anomalies (see fig. 3) exhibit a multistage history with two ridge jumps of the SEIR at 6.3 and 3.3 Ma [Courreges et al. submitted]. Maia and co-workers evaluated the crustal structure of the plateau using the calculated positions of the plume in the past and the rheology of the lithosphere, leading them to conclude that plume flux varied during construction of the plateau. Changes of its relative position to the SEIR could also account for the morphology changes and hence related magma flux variations. In other words, there were two periods of higher melt supply between 9.7 and 6.3 Ma and between 3.3 Ma and present, separated by a lower magmatic production stage. The on-axis major magmatic stage, responsible for the construction of the plateau is represented by three samples in our sample suite: PLU DR 6-1-1, PLU DR 6-2-2 and PLU DR 34-1-1. The northeastern part of the plateau, located on the Australian plate, contains a short volcanic chain of seamounts, which show a variety of morphologies from small volcanoes (PLU DR 10-1-1, PLU DR 10-2-2) to large seamounts (PLU DR 39-1-1/Rimbaud). They are either built on to the plateau or on its edge and represent a later off-axis magmatic stage. The difference between on- and off-axis magmatism is thus highlighted by the structure morphology with (1) on-axis magmatism building a

thicker oceanic crust and (2) off-axis magmatism occurring later and resulting into the construction of edifices on the oceanic bottom.

In this paper, we used K-Ar dating to constrain the ASP hotspot activity. We also used morphological features and some geochemical characteristics to further group events when geochronology data could not be used. It helped also to depict the influence of tectonic stresses during the construction of the ASP plateau and seamounts.

2. Structures and samples description

The modeled track of the ASP hotspot, which may represent the ASP plume activity prior its interaction with the SEIR, is parallel to the chain of seamounts located between 80°30E and 87°E, between the ASP and the Broken Ridge plateaus [Luyendyk et al., 1977; Royer et al., 1988]. This work will focus on the part of the chain located between 80°30E and 84°E (fig. 2). However, it is important to note that there is no evidence of an oceanic plateau at the beginning of the supposed ASP hotspot track, i.e., the initial plume activity does not reflect the impact of a plume head. From SW to NE, eight seamounts were identified: Apollinaire; Lamartine, Chateaubriand, Sand, Voltaire, La Bruyère, Boileau and La Fontaine. Together with the Ronsard and Du Bellay seamounts, located northward, they constitute the chain of the Dead Poets (CDP). The last two seamounts are not considered in this paper because of very incomplete bathymetric data and lack of fresh rock samples for geochemical analyses and age dating. Some morphological characteristics are summarized in table 1. The CDP is composed of two types of seamounts: those with steep summits and those with flat summits as seen in cross section (Fig. 4). Special attention has to be paid to Lamartine as its cross-section suggests a flat summit, but the digital elevation model (DEM) reveals that this seamount is composed of two distinct sharp summits.

Boileau and La Bruyère seamounts are special since they are the only two with a basal area greater than 800km² while all the other seamounts are smaller than 500km². This means that their volume is about 2 to 4 times greater, which combined with their flat summit profiles could indicate that those seamounts were above sealevel for some time, forming a volcanic island and then getting eroded and submerged again.

The morphology of the seamounts appears to be elongated with a length/width ratio larger than 1.4 for all but La Fontaine seamount. Both the chain and the long axis of the seamounts show a N65° orientation. This orientation, different from the SEIR N50° spreading direction, suggests at least a partial tectonic control on the seamount construction.

All the samples collected during the PLURIEL cruise and used in this study are presented in the table 2. The CDP samples are highly alkaline, reaching the tephrite/basanite compositions (Fig. 5 TAS diagram [LeBas et al., 1991]). In contrast, the plateau samples are mostly tholeiitic basalts except for the current SEIR samples, which are andesitic basalts. We report unpublished data from PLURIEL samples not used in this geochronological paper for comparison. Petrographically the CDP samples are richer in vesicles than the plateau samples but we have not noted any petrographic systematic variation with the location or the depth of the collected samples.

II. K-Ar geochronology

1. Procedure

1.1. Selection and Preparation of the samples

Eighteen samples were selected for geochronological study based on their distance from the ridge axis and their degree of alteration. Glassy samples were avoided because of possible excess argon caused by rapid quenching which impedes loss of the non-initial atmospheric argon [Dalrymple et al., 1968]. Major elements analyses were used to estimate the degree of alteration of the samples and to establish the rock type of the samples (Table 3). The K_2O vs. Nb ratio is a good indicator of alteration, whereby alteration would cause increases in K_2O for any given Nb value (Fig. 6). The K_2O and Nb values measured on whole rocks samples are reported in table 3. The good correlation between K_2O and Nb ($R^2 = 0.983$), and the generally (moderately) low L.O.I. values, confirms that the samples have not undergone significant post magmatic alteration. The loss-on-ignition value (L.O.I.) of these samples range from 0.01 to 1.11 % with an extreme sample with 3.44%. Based on its L.O.I sample PLU DR14-1-1 could be considered altered but the L.O.I. measurement were performed on the whole rock whereas K-Ar experiments were conducted on the cleaned groundmass. As detailed below alteration phases were removed mechanically and chemically. Since alteration phases on this sample were clearly aggregated in a small area, we are very confident in the separation of a cleaned groundmass.

After macroscopic and microscopic inspections, groundmass aliquots from fresh samples were prepared following the procedure described in Guillou et al. [1998]. The excess $^{40}Ar^*$ component can be partially avoided when processing only the well-crystallized interiors of submarine basalt flows [Dalrymple et al., 1968; Duncan et al., 1994]. All our samples were taken as far as possible (at least 4 cm) from the glassy rims of the pillows. The groundmass is assumed to have formed shortly after eruption and should not contain any excess $^{40}Ar^*$. All the samples were crushed and sieved to 0.250-0.125 mm size fractions and ultrasonically washed in acetic acid (1N) for 45 minutes at a temperature of 60°C, to remove any secondary

minerals phase that might be present in minute amounts. Phenocrysts and xenocrysts, which are potential carriers of extraneous $^{40}Ar^*$ (including excess and inherited components), were eliminated using magnetic, gravimetric and visual hand-picking separation.

1.2. Measurement

The unspiked K-Ar technique dynamically compares the isotopic composition of an aliquot of pure atmospheric Ar with the sample Ar composition to accurately determine minor variations of the $^{40}Ar/^{36}Ar$ isotopic ratio between the standard and the unknown. This method provides a precise correction for atmospheric Ar contamination and it avoids any discrimination effects of the mass spectrometric measurements [Cassignol&Gillot, 1982]. When compared to the $^{40}Ar/^{39}Ar$ method, this alternative method of conventional K-Ar dating has proven successful in dating very young typically subaerial rocks [Guillou et al., 1998; Ackert et al., 2003; Singer et al., 2004; Guillou et al., 2004].

The determination of K was carried out by atomic absorption with a relative precision of 1%. Argon was extracted by radio frequency heating of 0.4 to 1.8g of sample, then transferred to an ultra-high-vacuum glass line and purified with titanium sponge and Zr-Ar getters. The analyzed gases must be as pure as possible because active gases present in the mass spectrometer may react with the source filament and therefore change the ionization conditions. Helium, which can penetrate into the line when heating the titanium sponge, is eliminated via cryogenic pumping just before the introduction of the gases into the mass spectrometer. The atmospheric correction is monitored via two separate measurements of atmospheric Ar for each sample. A first atmospheric Ar aliquot (Air-1: reference dose) is measured at the same gas pressure as the sample, and serves as an isotopic reference for the determination of its radiogenic content under identical mass-discrimination conditions. The

second (Air-2: calibration dose) consists in a manometrically-calibrated dose of atmospheric Ar (from a separate reservoir of known ^{40}Ar content). This is used to convert beam intensities into atomic abundances. As both reference aliquots (isotopic and manometric) are atmospheric in composition, they provide a cross check on the radiogenic composition of the sample. Periodic cross calibration of zero-age standards precisely constrains the mass-discrimination to within 0.05‰ on the $^{40}Ar/^{36}Ar$ ratios [Scaillet&Guillou, 2004]

The manometric calibration of the Air-2 reference is based on repeated determinations of international dating standards of known K-Ar age using the same procedure for the samples to be analyzed as described in Charbit et al. [1998]. The total ^{40}Ar content of the sample is determined with a precision of about +/- 0.2% (2σ). Standards used include LP-6 (127.8 ± 0.7 Ma, (Odin et al., 1982) and HD-B1 (24.21± 0.32 Ma, Fuhrmann et al., 1987, Hess et al., 1994, Hautmann et al., 2000). At the 95% confidence level, the values adopted here are consistent with those obtained for several $^{40}Ar/^{39}Ar$ standards through the intercalibration against biotite GA-1550 by Renne et al. [1998] and Spell&McDougall [2003].

In principle, the most critical uncertainty in the K-Ar method is that it is not possible to verify the isotopic composition of the initial argon in the sample. That is, we cannot check the assumption that, at its time of formation, its $^{40}Ar/^{36}Ar$ ratio was the modern atmospheric value (295.5). As a result, the analytical errors given in Table 3 may in principle be less than the real error.

2. Results

Age determinations of the PLURIEL samples are reported in Table 3 and on figure 2. Analysis of each sample involved two determinations each of potassium and argon. The

potassium concentrations were combined to yield a mean value and its uncertainty. Separate age determinations were made using each of the argon measurements. The resulting ages and their uncertainties were then combined to yield an overall weighted mean estimate of the age of each sample and its uncertainty. Good analytical reproducibility of 40Ar* determination (see column 5, Table 3) is observed for all samples including the very young samples.

K-Ar ages are easily offset by alteration in particular, either leaching out K or adding it via recrystallisation to secondary (clay) minerals in the submarine basalts. The same processes may also cause a loss in $^{40}Ar^*$ resulting in higher apparent ages. Consequently, each result has to be confronted with geological constraints or by carrying out repeated analyses from the same rock, or even better yet by dredge samples collected from the same seamounts. All dated samples but one (PLU DR24-1-1) have Ar unspiked ages younger than the underlying crust which means they are geologically meaningful. This sample is dated at 5.56 +/- 0.14 Ma and according to the magnetic anomalies, it was formed on a 2 Ma old crust. Its K-Ar age is considered geologically meaningless and thus is discarded. As the sample material looked rather clean (L.O.I. of 0.29), the most likely explanation for this overestimated age is an excess of radiogenic $^{40}Ar^*$ in lava which was not totally degassed prior or during eruption. It is also possible to obtain a "too young" age. For unaltered samples with a low L.O.I, underestimation of K-Ar ages may come from bias in the experimental procedure. To limit this problem, each sample is analyzed twice, for K and Ar, on two completely separated procedures.

No radiogenic $^{40}Ar^*$ was detected in 4 samples (PLU DR 22-4-1, PLU DR 6-1-1, PLU DR 4-1-5, PLU DR 1-2-4) from the south central zone. These samples presumably are very young and define an area between the segment I2 of the SEIR and St Pierre seamount.

According to their K concentration, those samples should be younger than 0,1 Ma. Amsterdam and St Paul Island as well as Boomerang seamount are located close to this area. Based on paleomagnetic investigations (Watkins [1973 and 1975]) the building of these islands is considered to be contemporaneous with the Bruhnes period (< 780,000 years). St Paul Island activity has been dated between 20,000 and 40,000 years BP (Spiked K-Ar technique [Watkins et al., 1975]) as well as Amsterdam island late activity (Ar/Ar technique, [Carvallo et al., 2003]). Boomerang seamount activity is considered to be historical (eruption in 1995 - ^{210}Po-^{206}Pb [Johnson et al., 2000]).

III. Discussion

1. Origin of the chain of the Dead Poets

The CDP was regarded as the track of the ASP hotspot on the Australian plate [Luyendik et al., 1977] but our new isotopic ages do not confirm this assumption. Maia and co-workers [this issue] calculated with plate kinematic parameters the range of past positions of the ASP hotspot (Fig. 3). The hotspot past positions were computed considering a present location centered between Amsterdam and St. Paul islands. The relative movement between the hotspots and the Pacific are from Gripp&Gordon [2002] and between the Pacific and Antarctic-Australia from Cande&Stock [2004]. They assume that the past positions are probably well constrained between 6Ma and present. At 6 and 8 Ma the hotspot location is not as precisely constrained as <6 Ma, but a simple hotspot track model predicts that the CDP formed from 14 to 7 Ma.. La Fontaine (PLU DR 15), Lamartine (PLU DR 19) and Apollinaire (PLU DR 30) seamounts have K-Ar ages between 2.08 +/- 0.04 Ma (PLU DR 15) and 63 +/ 9 ka (PLU DR 30). These ages are much younger than the kinematically modeled ages, so either the K-Ar ages are underestimated or the seamounts are not related to the ASP hotspot activity. As mentioned before, underestimated K-Ar ages cannot be totally excluded due to technical

limitations. It seems however very unlikely to systematically underestimate all ages for all the seamounts. We can also exclude systematic datings of late-stage activity occurring several My after the main construction of the edifices. Indeed, Vergara Lopes [2009] performed a magnetic modeling on the seamounts of the CDP using the method of Maia et al. [2005]. The magnetic modeling of the young seamounts reveals that they do not exhibit mixed polarities while the geomagnetic polarity timescale for the last 10 My showed various inversion between normal and reverse polarity [Cande&Kent, 1995]. This suggesting that the main stage of construction of the young seamounts occurs within less than 1 My and then that they are formed from a process younger than the ASP hotspot intraplate activity.

Only one seamount, Boileau (PLU DR 14), dated at 8.37 +/- 0.18 Ma, fits with the 302 theoretical reconstruction and thus may correspond to the ASP plume activity on the Australian plate. The different phases of activity are summarized on the fig. 8. Its magnetic modeling reveals that Boileau seamount bears a normal magnetization, which is inconsistent with the 8.37 Ma age from our study that must have formed during reversed chron C4r.2r [Cande&Kent, 1995]. However, radiometric dating of seamounts is carried out on dredge samples, which are generally biased to a late phase of magmatism. The age of 8.37 Ma obtained for Boileau seamount suggest that the main volcanic phase of its construction occurred during the C4A normal chron, between 8.7 and 9.0Ma [Cande&Kent, 1995].

Boileau seamount age of 8.37Ma is compatible with the kinematic reconstruction of the ASP hotspot [Maia et al., this issue] and therefore with an origin directly linked to the hotspot. La Bruyère seamount, large and flat, may be as old as Boileau seamount and related to the ASP hotspot intraplate activity as well. This statement supports the assumption of a possible emerged stage for both of them since they are old enough to have grown above

sealevel and being eroded subsequently. Conversely, a different origin has to be found for the younger seamounts, which formed when the hotspot already had moved much closer to the current the SEIR. Consequently the CDP as a whole does not correspond to a single hotspot track as describe by Morgan [1972].

The CDP therefore results from at least two magmatic events leading to two generations of seamounts. The cause of that magmatic event can be either lithospheric, as consequence of a tectonic event, or deeper, as consequence of a pulse of the hotspot. The CDP exhibits a N65° orientation as well as the CDP seamounts. This elongated shape suggests a tectonic control on the seamounts construction. Boileau and La Bruyère seamounts distinguish from the others because of a larger size and a flat summit. Their larger size may be related to a higher degree of partial melting of the mantle, whereas the other seamounts would have erupted a smaller amount of melts. All the CDP samples are within or close to the tephrite field, regardless of age, which is not consistent with variations in the degree of partial melting through time. However, we cannot totally exclude such variations but it is likely that a longer period of activity and seamount construction should have generated the larger size of Boileau and La Bruyère seamounts.

We note that Apollinaire, Lamartine and La Fontaine seamounts are much younger (0.063 – 2.08 Ma) than Boileau seamount. Consequently, we assume that the small sharper seamounts Chateaubriand, Sand, and, Voltaire, sharing similar morphological characteristics may belong to this younger group.

All the seamounts have a N65° orientation, which means that despites their different sizes they share some morphological characteristics. This is suggesting that a common

tectonic event occurred at about 8 Ma (with Boileau construction) and lasted since 2 Ma (with the young seamounts construction). The magnetic modeling of the seamounts [Vergara Lopes, 2009] revealed that five seamounts exhibit a normal polarity and two are mixes of normal and reverse polarities. The mixed polarity of the geomagnetic polarity timescale for the last 10 My showed various inversion and a 1:1 repartition between normal and reverse polarity. This disagrees with the bias toward normal polarities recording the CDP seamounts suggesting that the construction of the CDP was not a continuous process. The two generations would then correspond to two "events" and not to a bias of sampling. Maia et al. [this issue] showed that ASP plume activity has not been regular but with pulses of higher magmatic activity and separated by a more or less quiet period. These two pulses have been recorded in the morphology of the ASP plateau and took place from 10 to 6 Ma ago and for the last 3 Ma. It is likely that the higher flux of material from the ASP plume extended laterally and ponded some material during the early stage of the plateau formation, leading to the construction of Boileau seamount. When a ridge and a plume come together most of the magmatism is driven toward the ridge melting zone but some of it can also be driven to the surface along stressed areas in the lithosphere. This area being in extension, a plume pulse can induce the construction of volcanoes away from the plateau, where the lithosphere is thinner and fragile. This process is related to the plume pulse and so it is expected to have occurred during the two periods of high magmatic production. This implies that the construction of the young seamounts should have occurred since 3 Ma, even if we collected no samples older than 2.08 +/- 0.04 Ma. The hotspot pulses induced the construction of the two generations of seamounts with a partial tectonic control so the maximum extension between Capricorn and Australian plates should be orthogonal to the associated volcanoes. Therefore, the N65° orientation of the chain and the seamounts constrains the maximum divergence as N155°. As there is no difference in the orientation of old and young seamounts, there seems to be no significant

variation of direction of divergence between the Capricorn and Australian plates for the last 8 Ma.

La Fontaine seamount is the only seamount that does not show an elongation. It is segmented from the other seamounts by the SPFZ, which offsets magnetic lineation about 10 My. Consequently, La Fontaine seamount is located on lithosphere 10 My older than that which underlies Lamartine, Apollinaire, and other seamounts. A 10 My older lithosphere is thicker and more robust and so may be less susceptible to deformations.

In summary, the timing and morphology of the seamounts is controlled both by the ASP plume activity and the regional lithospheric stresses induced by the plate motions. In addition, the plume pulses could act mechanically on the lithosphere to increase deformation and cause volcanic activity on the surface. This could especially be realistic for the 10-6Ma ASP hotspot pulse since the plume was closest to a deformed area. In fact, the source of the magmatism (ASP plume) was 400 km closer to the deformations field when Boileau and La Bruyère seamounts formed compared to the phase in which the younger seamounts were formed. Consequently, the amount of ponded plume material reaching the chain location would be higher for similar pulse intensity and would thus result in the construction of larger edifices.

The lithosphere was much older and thicker during the construction of the young seamounts than for the old ones (12 My old lithosphere against 7 My). This would have forced a deeper mantle melting which is consistent with the lower partial melting observed for the young seamounts. In conclusion, we assume that the old seamounts are larger because they formed closer to the hotspot through a greater degree of partial melting of the mantle

over a lithosphere that was more stressed and thus allowed for an easier pathway of the seamount magmas.

2. The ASP plateau as a product of the ASP plume-SEIR interaction

From the previous discussion we understand that magmatic activity has changed during the construction of ASP plateau as follows: (1) the first on-axis phase occurred when the SEIR and hotspot melting regions were connected resulting in the formation of the axial plateau, and (2) a second off-axis phase produced small volcanoes on the Australian plate in the northern part of ASP plateau. On- and off- axis samples are primarily tholeiitic basalt, as well as Amsterdam and St Paul Islands, which contrasts with the alkaline lavas recovered from the CDP (fig. 5). On- and off- axis samples thus derive from common (or similar) sources and processes. Our radiogenic ages compared with the calculated position of the hotspot in the past [see in Maia et al., this issue] and to the evolution of the SEIR axis position [Courreges et al.] allow us to describe the evolution of the geodynamical surrounding when on- and off-axis magmatic activity occurred.

PLU DR 8-1-1, PLU DR 10-1-1, PLU DR 10-2-2, PLU DR 28-1-1 and PLU DR39-1-1 are dated samples representing the off-axis activity of the plateau. We plotted the K-Ar ages of the off-axis volcanism samples (onto and outside the plateau) (y, in My) versus the current position of the ASP plume (between Amsterdam and St Paul islands, ([Royer et al. 1988] / x, in km) (Fig. 7a). With the exception of Rimbaud seamount (PLU DR 39), located on Amsterdam fracture zone, all the ages of the plateau systematically increase with the distance from Amsterdam and St Paul islands. Rimbaud seamount is located on Amsterdam FZ and is clearly bigger than the others seamounts located on the same FZ. Its construction occurred on a weak area, during a plume pulse period so it is likely that its construction have been

influenced by tectonic settings contrary to the other off-axis volcanoes located between fractures zones. Consequently, we excluded it from the discussion hereafter

We applied a level-headedness to the ages according to their distance from the plume to avoid bias toward the current hotspot activity. A linear correlation is observed, which equation is $y = 0.0107\ x$ for a correlation factor $R^2 = 0.963$. This linearity corresponds to the motion of the Capricorn and Australian plates considering they are moving together toward the NE. The calculated motion of the Capricorn-Australian block is of 9.3 cm/yr to the NE in a fixed plume model [Morgan 1972]. The SEIR is a ridge of intermediate spreading rate [Sempéré&Cochran, 1997; Conder et al. 2000], which on the I2 segment has an average of 5.94 cm/yr for the last 10 My [Courreges et al., submitted]. With a fixed Antarctic plate, this spreading rate concurs totally to the SEIR and the Capricorn-Australian block motions. Consequently, the apparent 9.3 cm/yr motion of the Capricorn-Australian block calculated with respect to a fixed ASP plume is too rapid to be due only to the spreading of the SEIR axis with a half-spreading rate of 2.97 cm/yr. Indeed, a motion of the Capricorn-Australian block only due to the SEIR spreading would be less than 6cm/yr. This velocity corresponds to a slope of 1/60 = 0,017; no edifices lie on this line (Fig. 7a). One explanation for this discrepancy could be that the ASP plume is not fixed. In that case, the absolute motion of the plume would be of about 3-4 cm/yr to the SW. However, this velocity is inconsistent with other hotspot motions like Hawaiian hotspot, which has been moving with a velocity of 1 cm/yr for the last 10 My [Kono, 1980; Tarduno et al., 2003; Duncan et al., 2006] as well as Indian Ocean hotspots [O'neill et al., 2003]. This overestimation results from the discrepancy between samples from off-axis edifices built on a fixed Antarctic plate and on a moving Capricorn-Australian. The deflection of the plume induced by the plate motions is thus different between the two sets of samples. If we remove all the ages of Antarctic plate

edifices, the correlation becomes $y = 0.0129 x – 1.249$ for a correlation factor $R^2 = 0.988$ (fig. 7b). The non-zero intercept translate the deflection of the plume toward the NE in response to the overlying plate movement, when compared to a centered-plume activity. The off-axis edifices of the Capricorn-Australian plate are thus shifted of about 100 km ($x = 96$ km for $y = 0$) when compared to the position of ASP plume at the time of the eruption. Considering the currently accepted plume "diameters" (150 km – Ito et al., 1997; Wolfe et al., 1997], and considering that ASP is probably a small hotspot of with a diameter of about 80 km [Maia et al., this issue], this shift is perfectly understandable and does not affect the slope of the observed correlation between K-Ar ages of the off-axis volcanism samples and the current position of the ASP plume. This correlation thus provides a 7.7 cm/yr motion of the Capricorn-Australian block, which is also too rapid to be due only to the spreading of the SEIR. This correlation thus provides 1-2 cm/yr motion to the SW of ASP plume, which is consistent with other hotspots motions. Therefore, we assume that the ASP plume motion is about 1-2 cm/yr to the SW

O'neill et al. [2003] calculated the motion of the Indian hotspots employing a plate motion revised and a tomography model to calculate mantle flow through time. They provided modeled motions consistent with the paleolatitutes estimates for the Kerguelen and Réunion hotspot. They also calculated ASP hotspot of the last 120Ma but could not constraint it with measured paleolatitutes. Their modeling suggests a motion to north between 120 and 60 Ma and to south at since 60 Ma, with an average velocity of 0.28cm/yr. Nevertheless, the discrepancy with our conclusions does not exclude any model since their calculations concern a motion though 120 My and ours for that last 10 My. The changing motion at about 60 Ma precludes a constant velocity though time. The average velocity given by O'neill et al. [2003] is thus compatible with our data.

A plot of K-Ar ages vs. age of the underlying crust (fig. 7c) provides an estimate of the motion of the SEIR relative to the hotspot. In order to calculate a more precise motion vector, we added a sample from Boileau since it is also related to the off-axis activity of the ASP hotspot. We observe a linear correlation, which equation is $y = 0.648 x - 0.717$ for a correlation factor $R^2 = 0.976$, with y corresponding to the age of the off-axis volcanoes (in Ma) and x the age of the underlying crust (in Ma). The age of the underlying crust is directly related to the distance from the ridge. Courreges and co-workers suggested that the average half-spreading rate of segment I2 is 2.97 cm/yr during the period of the plateau construction. Using this information, we can convert the age of the underlying crust into the distance from the SEIR at the time of the off-axis volcano construction and plot the off-axis volcanoes (y, in Ma) versus their distance to the SEIR (x, in km). The correlation observed then becomes $y = 0.054 x - 1.298$ with a correlation factor $R^2 = 0.823$. The inverse of the slope, $1/0.054 = 18.5$ corresponds to the relative motion between the SEIR and ASP plume in km/Ma. In other words, the SEIR and the ASP seem to have converged with a velocity of 1.85 cm/yr. This relative motion is the vectorial sum of the absolute motions of the SEIR itself, the ASP plume and the Antarctic plate. All those motions have been reported on the fig. 8 cartoon. Considering the Antarctic plate as fixed, the SEIR moving from SW to NE at 6 cm/yr and the ASP plume moving from NE to SW at 1-2 cm/yr, the relative convergence of 1.85 cm/yr between the SEIR and the plume is too small to be realistic. This means that the motion of the SEIR has not been continuous to the NE during this period. Those results confirm then the SEIR jumps to the SW evidenced by Maia et al. [this issue].

Behn et al. [2004] suggested that a strong asthenospheric flow is moving away from Africa (superswell). In this case, the ridge and the plume would be moving to the East and the

apparent motion of the Capricorn-Australian plate vs. the hotspot would be lower than the SEIR half-spreading rate creating the I2 plate segment. Conversely, Steinberger [2000] calculated the deformation of plumes deep-seated conduit in order to estimate the surface hotspots tracks. He evidenced that plume conduits were tilted toward large upwellings because of the lower mantle flow. In this case, the hotspot surface motion often represents the horizontal component of the mid-mantle flow, generally opposite to the plate motion. The ASP plume, however, is moving toward the SW. This means that ASP plume has been moving toward the ridge, toward the large African superswell and thus against the asthenospheric flow. This movement thus requires a deep-seated conduit, which suggests that ASP plume origin is located in the lower mantle.

Zhao [2007] provides tomographic images under sixty major hotspot, including ASP. They evidence continuous low velocity anomalies in both upper and lower mantle visible under ASP plateau, suggesting that ASP hotspot could be originating from the core-mantle boundary. This is in agreement with the deep-seated conduit evidenced here. In addition, the tilted images of the so-called ASP plume toward Africa consolidate Steinberger's conclusions and thus ours.

IV. Conclusion

This study showed that the ASP hotspot activity and interaction with the SEIR is complex. The geochronological constraints of the various phases of activity allow an evaluation of the relative and absolute motion of the plates and the plume involved in the system.

First, the chain of seamounts considered as the ASP plume intraplate activity is made of two generations of seamounts, related to both ASP plume activity and regional tectonic

settings: (1) large edifices were formed between 10 and 8 Ma, which possibly reached the surface as evidenced by their flat summit, and (2) smaller edifices were constructed over the past 2-3 My. The ASP plume is a small plume, which expresses onto a weak lithosphere and in a non regular way through time. The construction of the CDP is then due to the conjunction of the plume pulse and of stresses at the Capricorn-Australian diffuse boundary, leading melts toward the surface. The elongated shape of the seamounts of the CDP indicates that the maximum deformation between Australian and Capricorn plates occurred along a N155° direction for the last 10 Ma. The conjunction of plume pulse on a weak lithosphere also induced the construction of volcanic edifices (like Rimbaud seamount) on the ASP plateau.

Secondly, the apparent velocity of the Capricorn-Australian block northeastwards does not fit with a fixed-plume model Morgan [1972]. We assume that the ASP plume motion is about 1-2 cm/yr to the SW. This motion in the opposite direction of the atshenospheric flow requires deep-seated anchorage of the conduit and so a deep origin for ASP plume.

Finally, the relative convergence calculated between the SEIR and the plume is inconsistent with a continuous movement of the SEIR toward NE for the last 10 My, confirming then the SEIR jumps to the SW evidenced by Maia et al. [this issue] during this period..

Acknowledgments:

We thank Captain Duchesne, the crew of the "Marion Dufresne II" and the PLURIEL scientific party for their help with the acquisition and treatment of the data. This manuscript benefited from constructive comments from A. Hofmann and J. Dyment. We are also indebted to F. Frey and A. Koppers who helped improve the manuscript.

The PLURIEL cruise was funded by the "Centre National de la Recherche Scientifique – Institut Nationale des Sciences de l'Univers" through the program SEDIT, by IPEV and by the program EXTRAPLAC.

References:

Ackert, R.P., Singer, B., Guillou, H., Kaplan M.R., Kurz, M.D., (2003). Cosmogenic ^{3}He production rates from 40Ar/39Ar and K-Ar dated Patagonian lava flows at 47ES. *Earth Planet. Sci. Lett. 219,* 119-136.

Behn, M. D., Conrad, C. P., Silver, P. G., (2004). Detection of upper mantle flow associated with the African Superplume. *Earth Planet. Sci. Lett. 224,* 259-274.

Cande, S. C., Kent, D. V., (1995). Revised calibration of the geomagnetic polarity time scale for the Late Cretaceous and Cenozoic. *J. Geophys. Res. 100*, 6093-6095.

Carvallo, C., Camps, P., Ruffet, G., Henry, B., Poidras, T., (2003). Mono Lake or Laschamp geomagnetic event recorded from lava flows in Amsterdam Island (southeastern Indian Ocean). *Geophys. J. Int. 154,* 767-782.

Cassignol, C., Gillot, P.Y., (1982). Range and effectiveness of unspiked potassium-argon dating: experimental groundwork and applications. *In: Odin, G.S. (Ed), Numerical Dating in Stratigraphy. Wiley, 1*, 159-179.

Charbit, S., Guillou, H., Turpin, L., (1998). Cross calibration of K-Ar standard minerals using unspiked Ar measurement technique. *Chem Geol. 150*, 147-159.

Conder, J. A., Forsyth, D. W. (2001) Seafloor spreading on the Southeast Indian Ridge over the last one million years: a test of the Capricorn plate hypothesis. *Earth Planet. Sci. Lett. 188*, 91-105.

Courreges, E., Maia, M., Patriat, M., Pessanha, I., Roest, W., Royer, J.-Y., (2010). Evolution of ridge segmentation on the St-Paul&Amsterdam Plateau from 10 Ma, in the context of ridge-hotspot interaction. Submitted to *Journal of Geophysical Research.*

Dalrymple, G.B., Lanphere, M.A., (1968). Potassium-Argon dating. Principles Techniques and Applications to Geochronology. *W.H. Freeman and company, San Francisco.* (251 pp).

DeMets, C., Gordon, R. G., Argus, D. F., (1988). Intraplate deformation and closure of the Australia-Antarctica-Africa plate circuit. *J. Geophys. Res. 93*, 11877-11897.

Doucet, S., Weis, D., Scoates, J.S., Debaille, V., Giret, A., (2004). Geochemical and Hf-Pb-Sr-Nd isotopic constraints on the origin of the Amsterdam-St. Paul (Indian Ocean) hotspot basalts. *Earth Planet. Sci. Lett. 208*, 179-195.

Duncan, R.A., Hogan, L.G., (1994). Radiometric dating of young MORB using the $^{40}Ar/^{39}Ar$ incremental heating method. *Geophys. Res. Lett. 21(1*8), 1927-1930.

Duncan, R. A., Tarduno, J. A., Scholl, D. W., (2006). Leg 197 Synthesis: Southward motion and geochemical variability of the Hawaiian Hotspot. *In: Proceedings of the Ocean Drilling Program, Scientific Results. R. A. Duncan, J. A. Tarduno, T. A. Davies and D. W. Scholl*.

Fuhrmann, U., Lippolt, H., Hess, C.J., (1987). HD-B1 biotite reference material for K-Ar chronometry. *Chem. Geol. 66*, 41-51.

Gente P. Dyment J., Maia M, Goslin J., (2003). The Azores plateau: an example of hot-spot/Ridge interaction. Geochem. Geophys. Geosyst., 4(10), 8514, doi:10.1029/2003GC000527.

Girot, M., Camus, G., Vialette, Y., (1971). Sur la présence de tholéiites à l'île St Paul (Océan Indien). *Contr. Mineral. And Petrol. 33*, 108-117.

Gripp, A. E., Gordon, R. G., (1990). Current plate velocities relative to the hotspots incorporating the NUVEL-1 global plate motion model. *Geophys. Res. Lett.* 17, 1109-1112.

Guillou, H., Carracedo, J.C., Day, S., (1998). Dating the upper Pleistocene-Holocene volcanic activity of La Palma using the Unspiked K-Ar technique. *J. Volcan. Geoth. Res. 86*, 137-149.

Guillou, H., Singer, B., Laj, C., Kissel, C., Scaillet, S., Jicha, B.R., (2004). On the age of the Laschamp geomagnetic event. *Earth Planet. Sci. Lett. 227*, 331-343.

Gunn, B.M., Abranson, C.E., Nougier, J., Watkins, N. D., Hajash, A., (1971). Amsterdam Island, an isolated volcano in the southern Indian ocean. *Contr. Mineral and Petrol., 32*, 79-92.

Gunn, B. M., Watkins, N. D., Trzcienski, W. E. Jr., Nougier, J., (1975). The Amsterdam-St Paul volcanic province and the formation of low Al tholeetic andesites. *Lithos 8*, 137-149.

Hautmann, H.J., Lippolt, H., (2000). 40Ar/39Ar dating of central European K-Mn oxides, a chronological frameworkof supergene alteration processes during the Neogene. *Chem. Geol. 170*, 37-80.

Hess, C.J., Lippolt, H., (1994). Compilation of K-Ar measurements on HD-B1 standard biotite. *In Odin, G.S. (Ed), Phanerozoic Time Scale Bull. Liais. Inform. I.U.G.S, Subcom. Geochronol*., pp 19-23;

Johnson, K.T.M., Graham, D.W., Rubin, K.H., Nicolaysen, K., Scheirer, D.S., Forsyth, D.W., Baker, E.T., Douglas-Priebe, L.M., (2000). Boomerang Seamount: the active expression of the Amsterdam-St. Paul hotspot, Southeast Indian Ridge, *Earth Planet. Sci. Lett. 183*,245-259.

Kono, M., (1980). Paleomagnetism of DSDP Leg 55 basalts and implications for the tectonics of the Pacific Plate. Init. Rep. Deep Sea Drill Proj. 55, 737-752.

Le Bas, M. J., Le Maitre, R. W., Woolley, A. R., (1991). The construction of the Toral Alkali-Silica chemical classification of volcanic rocks. Mineralogy and Petrology 46(1), 1-22.

Luyendik, B.P., Rennick, W., (1977). Tectonic history of aseismic ridges in the eastern Indian Ocean, *Geol. Soc. Am. Bull. 88*, 1347-1356.

Maia, M., Dyment, J., Jouannetaud, D., (2005). Constraints on age and construction process of the Foundation chain submarine volcanoes from magnetic modeling. *Earth Planet. Sci. Lett. 235*,283-299.

Maia, M., Courreges, E., Pessanha, I., Hemond, C., Janin, M., Bassoullet, C., Brachet, C., Chavrit, D., Gente, P., Humler, E., Johnson, K., Loubrieu, B., Martin, C., Mudholkar, A., Oldra, J., Patriat, M., Raquin, A., Richard, M., Royer, J., Vatteville, J., (2008). Evolution of the Saint Paul Amsterdam Plateau in the Last 10 m.y. *Eos Trans. AGU, 89*(53), Fall Meet. Suppl., Abstract T54B-06.

Maia, M., Pesshana, I., Courreges, E., Patriat, M., Gente, P., Hemond, C., Janin, M., Johnson, K., Roest, W., Royer, J.-Y., Vatteville, J., (2010). Building of the Amsterdam-St. Paul plateau: a 10 Myr history of a ridge-hotspot interaction and plume pulses. In revision for *Journal of Geophysical Research*. Doi: 10.1029/2010JB007768

Minster, J., and T. Jordan (1978), Present-day plate motions, J. Geophys. Res., 83(B11), 5331-5354.

Morgan, W.J., (1972). Deep mantle convection plumes and plate motions, *Bull. Am. Assoc. Pet. Geol.*, 56, 203-213.

Nicolaysen, K. P., Frey, F. A., Mahoney, J. J., Johnson, K. T. M., Graham, D.W., (2007). Influence of the Amsterdam/St. Paul hot spot along the Southeast Indian Ridge between 77°

and 88°E: Correlations of Sr, Nd, Pb and He isotopic Variations with ridge segmentation, *Geochem. Geophys. Geosyst., 8*, Q09007, doi:10.1029/2006GC001540.

Odin, G.S., (1982). Interlaboratory standards for dating purposes. *In: Odin, G.S. (Ed), numerical dating in stratigraphy. Wiley, Chichester*, pp. 123-150.

O'neill, C., Müller, D., Steinberger, B., (2003). Geodynamic implications of moving Indian Ocean hotspots. *Earth Planet. Sci. Lett. 215*,151-168.

Renne, P.R., Swisher, C.C., Deino, A.L., Karner, D.B., Owen, T.L., DePaolo, D.J., (1998). Intercalibration of standards, absolute ages and uncertainties in $^{40}Ar/^{39}Ar$ dating. *Chem. Geol. 145*, 117-152

Royer, J.Y., Schlich, R., (1988). Southeast Indian Ridge between the Rodriguez Triple Junction and the Amsterdam and St. Paul Islands: detailed kinematics for the past 20 m.y., *J. Geophys. Res. 93 (B11)* 13524-13550.

Royer, J. Y., Gordon, R. G., (1997). The motion and boundary between the Capricorn and the Australian plates. *Science. 277,* 1268-1274.

Scaillet, S., Guillou, H., (2004). A critical evaluation of young (near-zero) K-Ar ages. *Earth. Planet. Sci. Lett. 220*, 265-275.

Schilling, J.-G., (1973). Iceland Mantle plume: geochemical study of Reykjanes ridge. *Nature, 314*, 62-67

Schilling, J-G., (1991). Fluxes and excess temperatures of mantle plumes inferred from their interaction with migrating mid-ocean ridges, *Nature, 352*, 397-403.

Sempéré, J. C., Cochran, J. R. (1997). The Southeast Indian Ridge between 88°E and 118°E : Variations in crustal accretion at constant spreading rate. *J. Geophys. Res*. 102(B7), 15,489-15,505.

Singer, B.S., Ackert, R.P., Guillou, H., (2004). $^{40}Ar/^{39}Ar$ and K-Ar geochronology of Pleistocene glaciations in Patagonia, *Geol. Soc. Am. Bull. 116*, 434-450.

Spell T.L., McDougall, I., (2003). Characterization and calibration of $^{40}Ar/^{39}Ar$ dating standards. *Chem Geol. 198*, 189-211.

Steiger, R.H., Jäger, E., (1977). Subcommission on geochronology: convention of the use of decay constants in geo and cosmochronology. *Earth Planet. Sci. Lett. 36*, 359-352.

Stein, S., Gordon, R. G., (1984). Statistical tests of additionale plate boundaries from plate motion invertions. *Earth Plan. Sci. Lett. 69*. 401-412.

Steinberger, B., (2000). Plumes in a convecting mantle: models and observations from individual hotspots. *J. Geophys. Res. 105(B5)*, 11, 127-11,152.

Tarduno, J. A., Duncan, R. A., Scholl, D. W., Cottrell, R. D., Steinberger, B., Thodarson, T., Kerr, B. C., Neal, C. R., Frey, F. A., Torii, M., Carvallo, C., (2003). The Emperor Seamounts: Southward motion of the Hawaiian hotspot plume in Earth's mantle. *Science 301*, 1064-1069.

Vergara Lopes, P., (2009). Modelagem magnetic dos vulcoes do alinhemento dos Poetas Desaparecidos. Relatorio de estagio de Iniciacao Cientifica, Universidade Federal Fluminense e IUEM.

Vogt, P.R., (1976). Plumes, subaxial pipe flow and topography along the mid-oceanic ridge. *Earth Plan. Sci. Let., 29*, 309-325

Watkins, N. D., Nougier, J., (1973). Excursions and secular variation of the Bruhnes epoch geomagnetic field in the Indian Ocean region. *J. Geophys. Res. 78*, 6006.

Watkins, N.D., McDougall, I., Nougier, J. (1975). Paleomagnetism and potassium-argon age of St. Paul Island, southeastern Indian Ocean: contrasts in geomagnetic secular variation during the Brunhes Epoch, *Earth Planet. Sci. Lett. 24*, 377-384.

Wiens, D. A., DeMets, C., Gordon, R. G., Stein, S., Argus, D., Engeln, J. F., Lundgren, P., Quible, D., Stein, C., Weinstein, S., Woods, D. F., (1985). A diffuse plate boundary model for Indian Ocean tectonics. *Geophys. Res. Lett. 12*, 429-432.

Zhao, D., (2007). Seismic images under 60 hotspots: search for mantle plumes. *Gondwana Research 12, 335-355*.

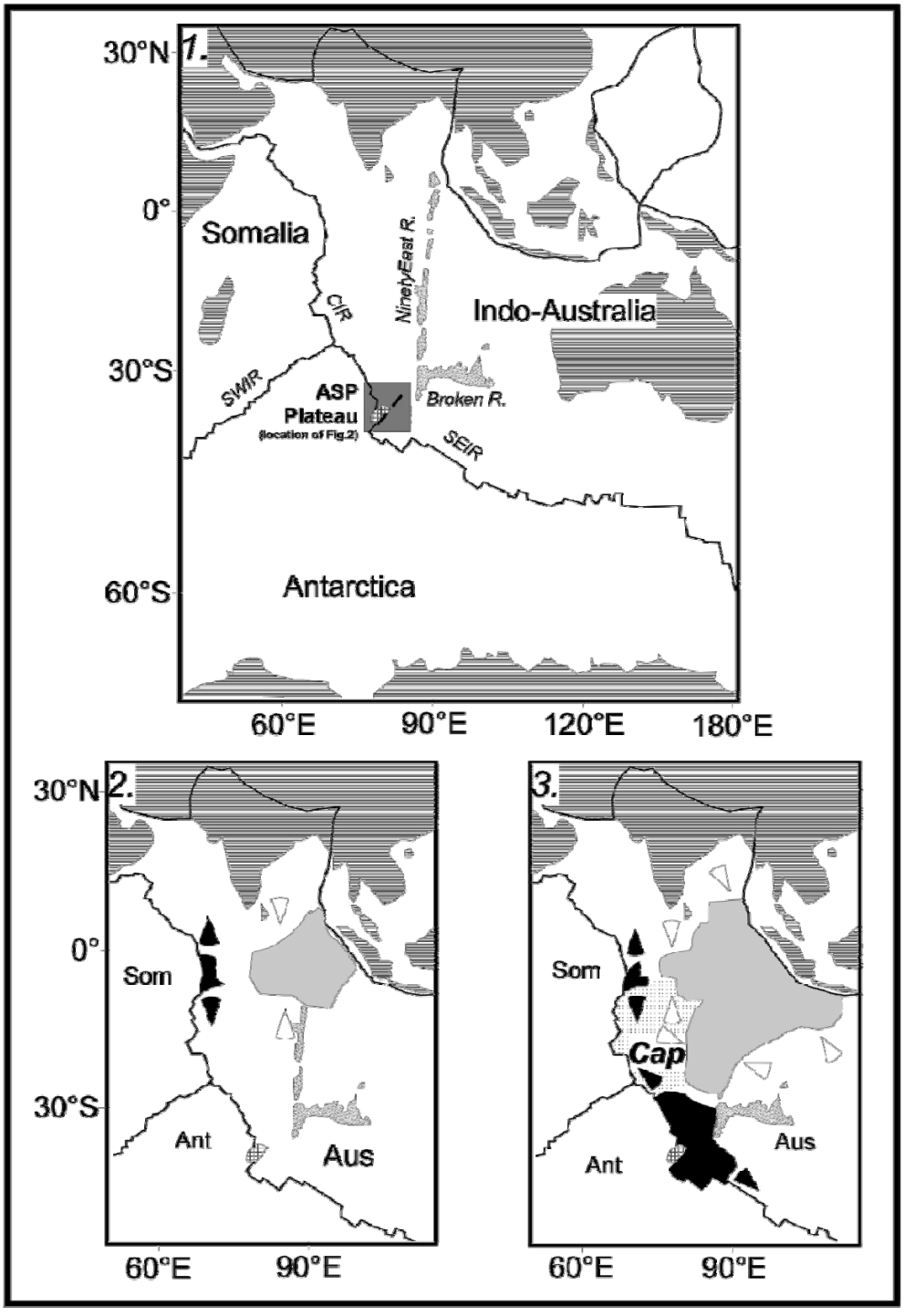
1.
30°N
0°
30°S
60°S
Somalia
CIR
Ninety East R.
Indo-Australia
SWIR
ASP
Plateau
(location of Fig.2)
Broken R.
SEIR
Antarctica
60°E
90°E
120°E
180°E
2.
30°N
0°
30°S
Som
Ant
Aus
60°E
90°E
3.
Som
Cap
Ant
Aus
60°E
90°E

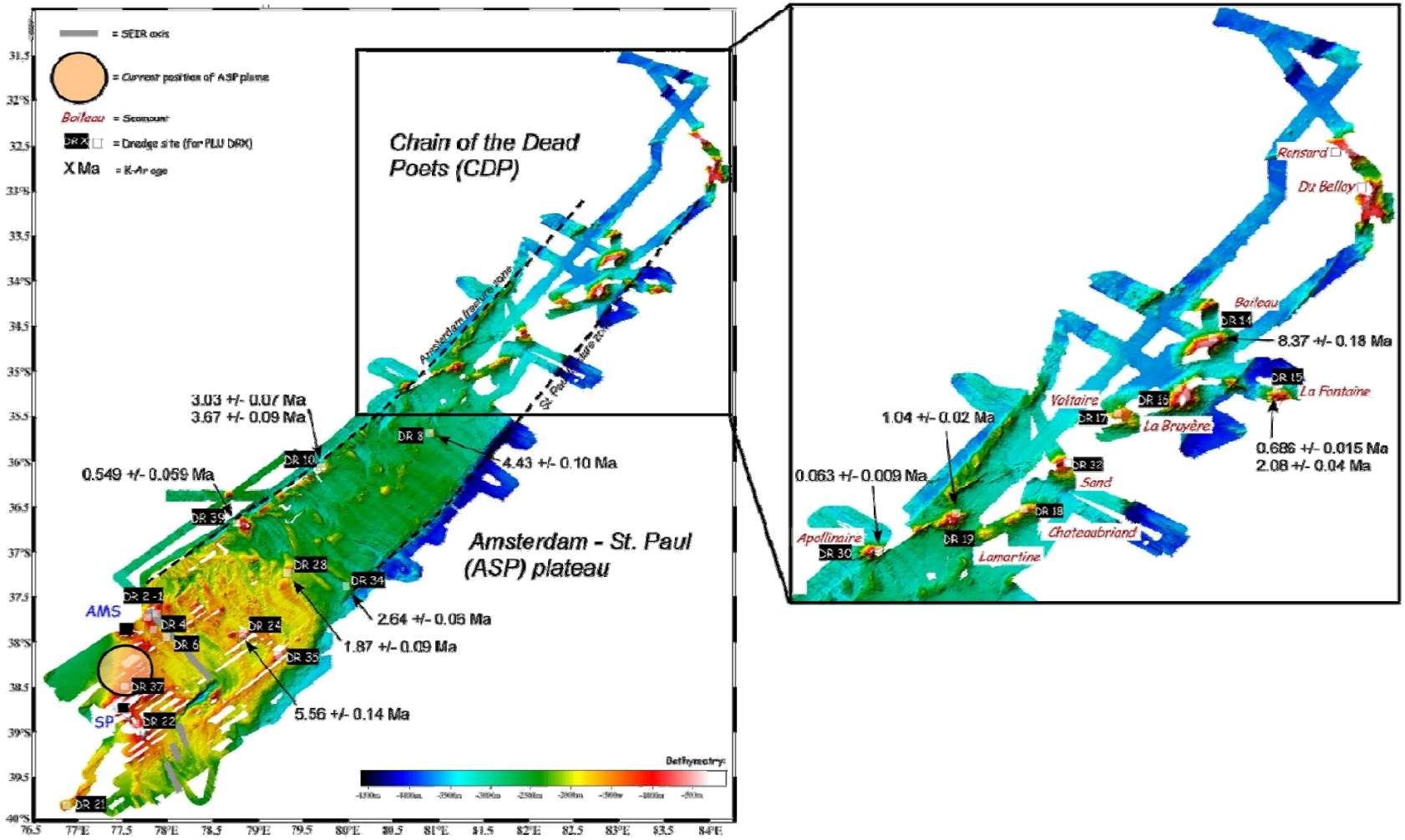
= SEIR axis
= Current position of ASP plume
Boileau = Seamount
DR X = Dredge site (for PLU DRX)
X Ma = K-Ar age
Chain of the Dead Poets (CDP)
Amsterdam fracture zone
St Paul fracture zone
Amsterdam - St. Paul (ASP) plateau
3.03 +/- 0.07 Ma
3.67 +/- 0.09 Ma
0.549 +/- 0.059 Ma
4.43 +/- 0.10 Ma
2.64 +/- 0.05 Ma
1.87 +/- 0.09 Ma
5.56 +/- 0.14 Ma
AMS
SP
DR 1
DR 2
DR 3
DR 4
DR 6
DR 10
DR 21
DR 22
DR 24
DR 28
DR 34
DR 35
DR 37
DR 39
Bathymetry:
Ronsard
Du Bellay
Boileau
DR 14
8.37 +/- 0.18 Ma
DR 15
La Fontaine
Voltaire
DR 16
DR 17
La Bruyère
1.04 +/- 0.02 Ma
0.686 +/- 0.015 Ma
2.08 +/- 0.04 Ma
0.063 +/- 0.009 Ma
DR 32
Sand
DR 18
Chateaubriand
Apollinaire
DR 19
DR 30
Lamartine

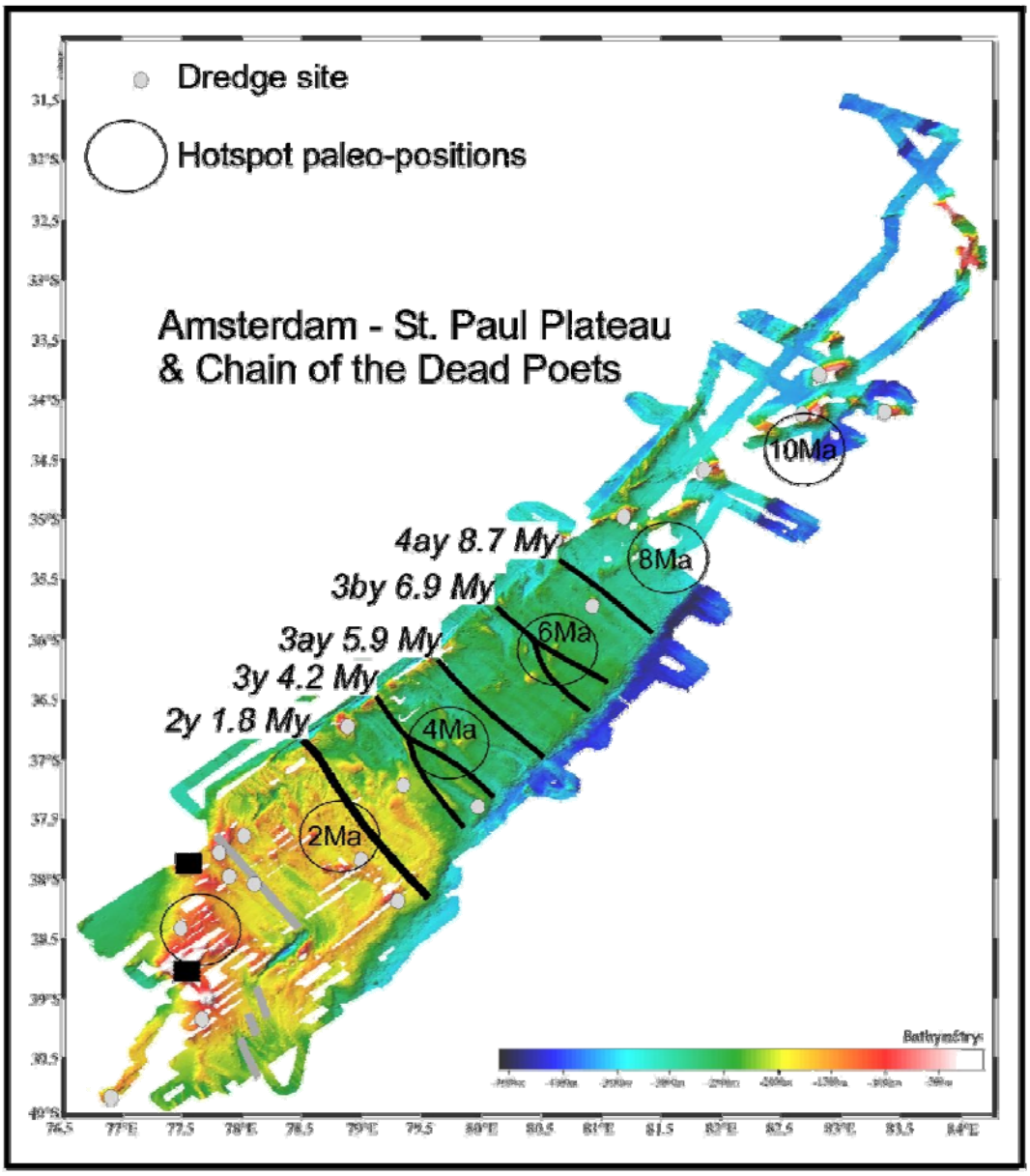
Dredge site
Hotspot paleo-positions
Amsterdam - St. Paul Plateau
& Chain of the Dead Poets
10Ma
8Ma
6Ma
4Ma
2Ma
4ay 8.7 My
3by 6.9 My
3ay 5.9 My
3y 4.2 My
2y 1.8 My
Bathymetry

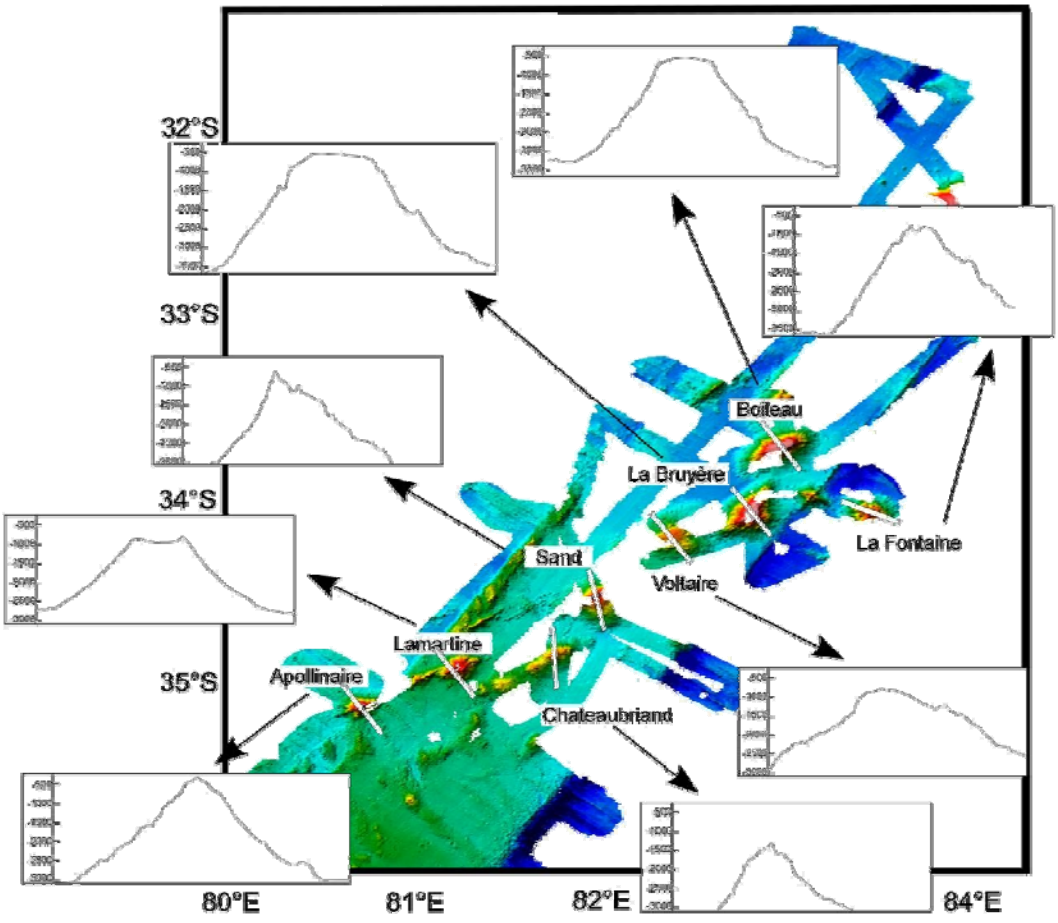
32°S
33°S
34°S
35°S
80°E
81°E
82°E
84°E
Boileau
La Bruyère
La Fontaine
Sand
Voltaire
Lamartine
Apollinaire
Chateaubriand

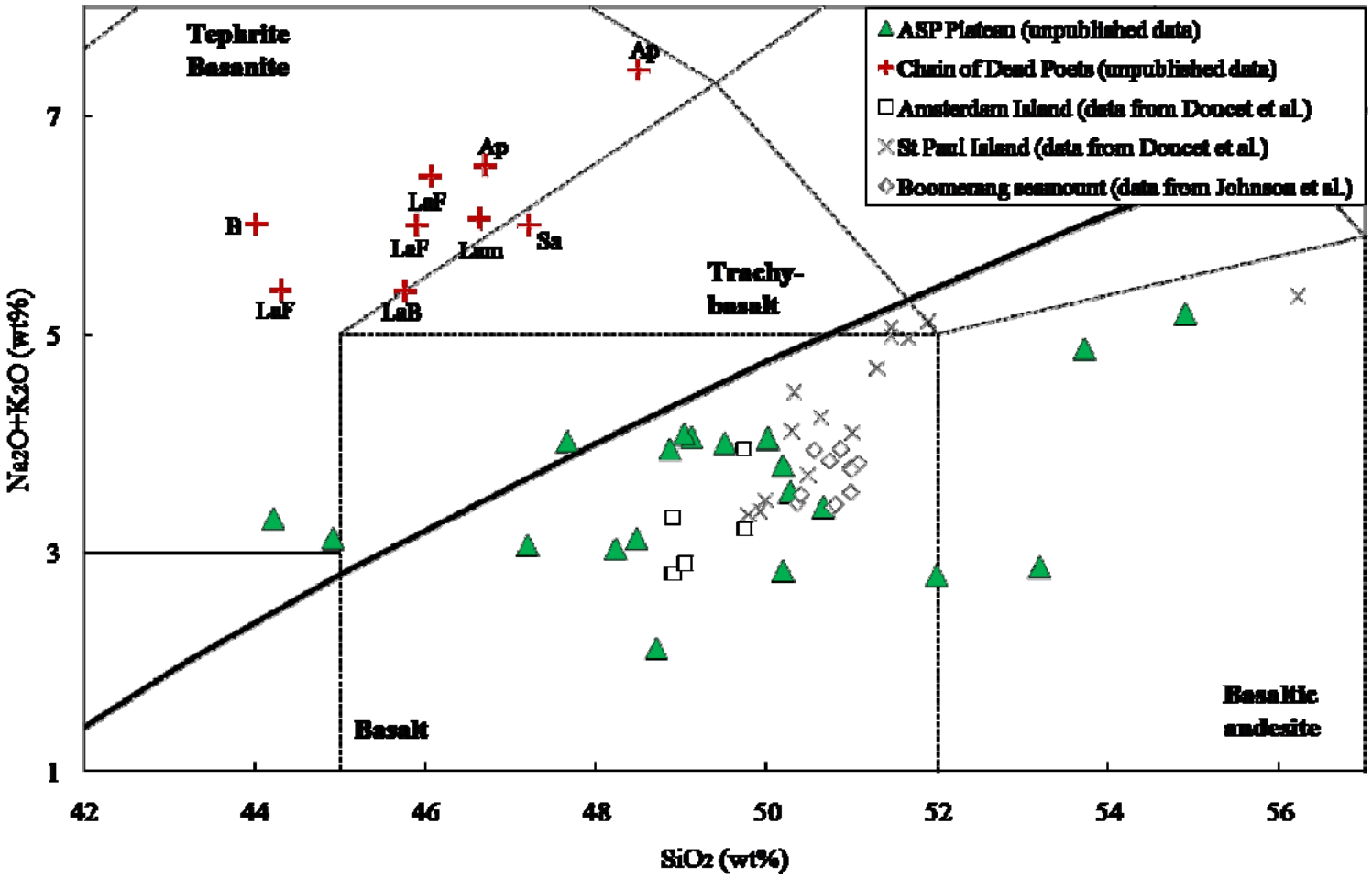
Tephrite
Basanite
Trachy-
basalt
Basalt
Basaltic
andesite
Ap
Ap
LaF
B
LaF
LaF
Lam
Sa
LaB
ASP Plateau (unpublished data)
Chain of Dead Poets (unpublished data)
Amsterdam Island (data from Doucet et al.)
St Paul Island (data from Doucet et al.)
Boomerang seamount (data from Johnson et al.)
Na2O+K2O (wt%)
SiO2 (wt%)
1
3
5
7
42
44
46
48
50
52
54
56

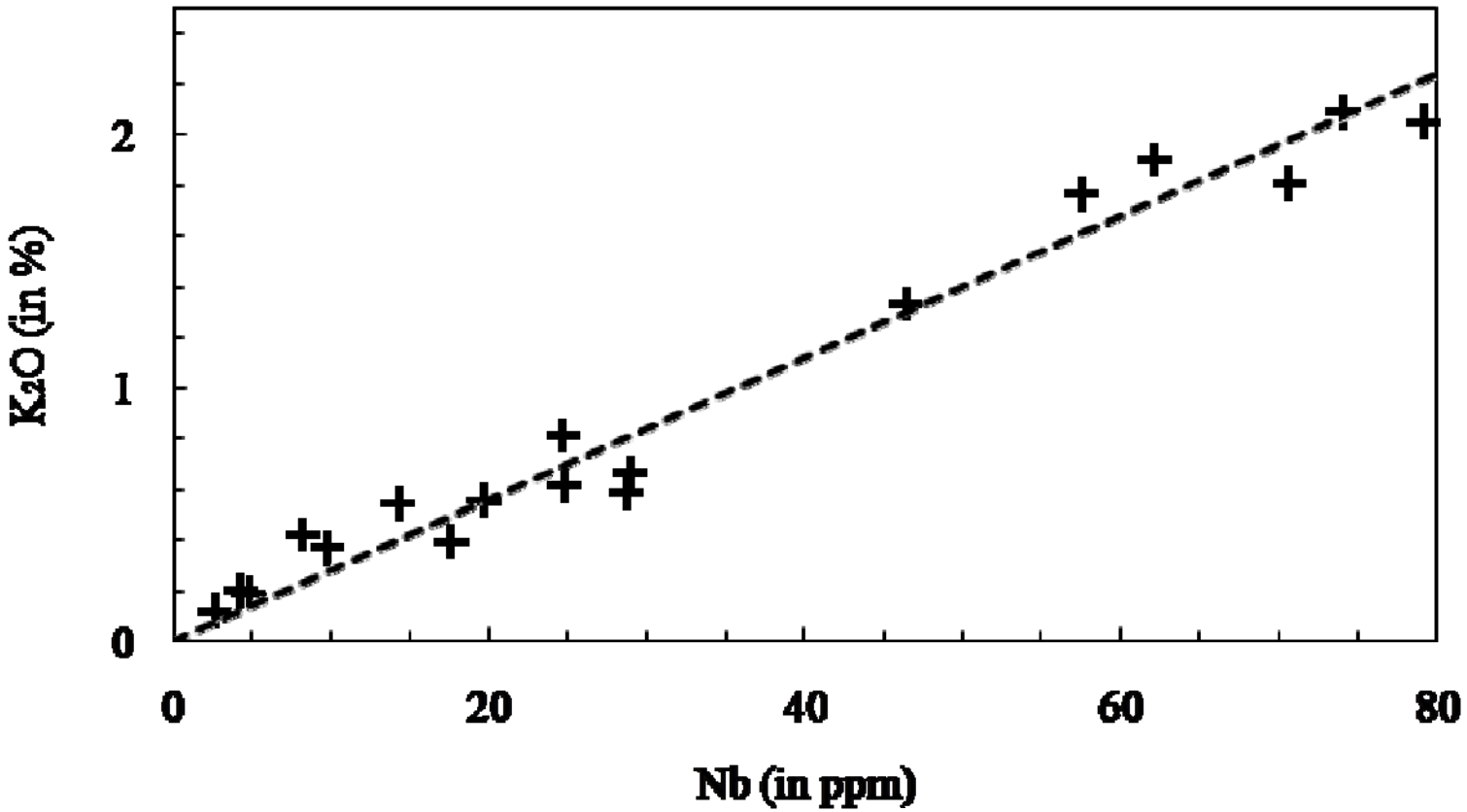
K2O (in %)
2
1
0
0
20
40
60
80
Nb (in ppm)

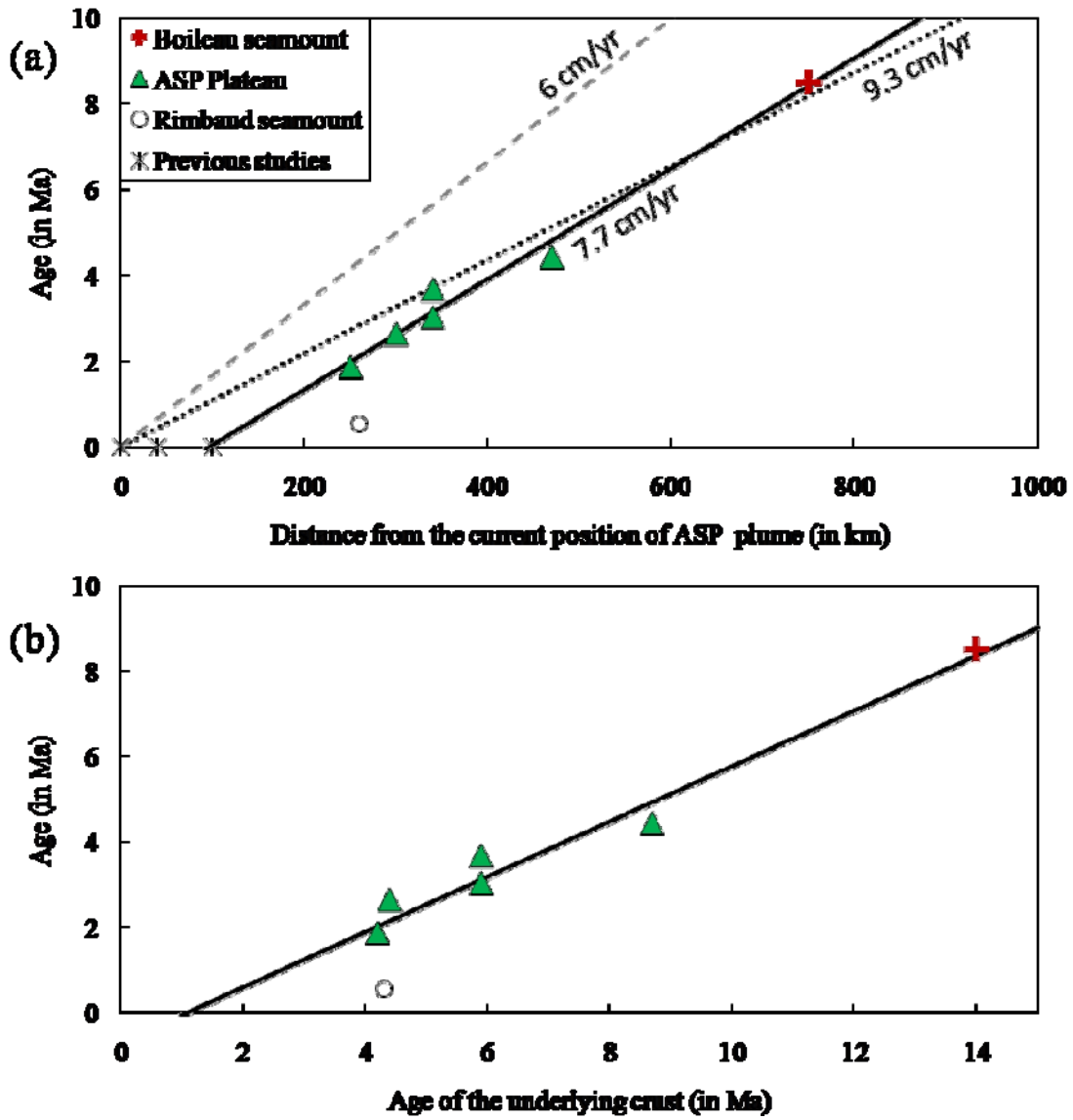
(a)
Hoilcau seamount
ASP Plateau
Rimband seamount
Previous studies
6 cm/yr
9.3 cm/yr
7.7 cm/yr
Age (in Ma)
Distance from the current position of ASP plume (in km)
0
2
4
6
8
10
0
200
400
600
800
1000
(b)
Age (in Ma)
Age of the underlying crust (in Ma)
0
2
4
6
8
10
12
14

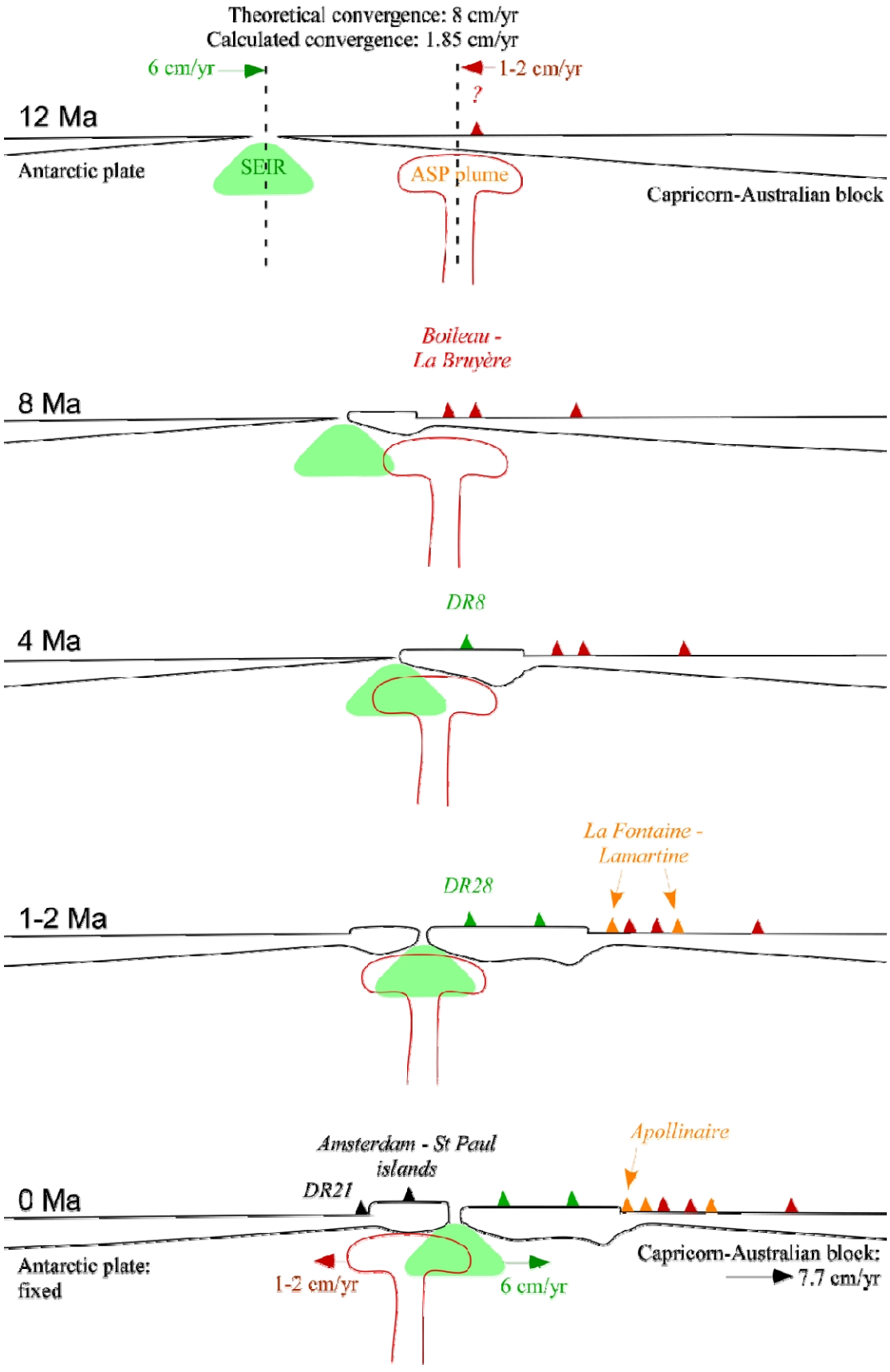
Theoretical convergence: 8 cm/yr
Calculated convergence: 1.85 cm/yr
6 cm/yr
1-2 cm/yr
?
12 Ma
Antarctic plate
SEIR
ASP plume
Capricorn-Australian block
Boileau - La Bruyère
8 Ma
DR8
4 Ma
La Fontaine - Lamartine
DR28
1-2 Ma
Amsterdam - St Paul islands
Apollinaire
DR21
0 Ma
Antarctic plate: fixed
1-2 cm/yr
6 cm/yr
Capricorn-Australian block:
7.7 cm/yr

Author version: J. Geophys. Res. (B: Solid Earth), vol.116(5); 2011; 17 pp; doi:10.1029/2010JB007800

Seamount	L = length (km) W = width (km)	Height (km)	Base area (km²)	Summit	Orientation (N°)
Apollinaire (PLU DR30)	L = 24 W = 16	2.7	325		65
Lamartine (PLU DR19)	L = 23 W = 16	2.1	280		65
Chateaubriand (PLU DR 18)	L = 36 W = 21	1.9	580		65
Sand (PLU DR32)	L = 35 W = 25	2.5	490		65
Voltaire (PLU DR17)	L = 30 W = 18	1.8	400		60
La Bruyère (PLU DR16)	L = 40 W = 27	3.3	800	flat	55
Boileau (PLU DR14)	L = 42 W = 24	2.9	900	flat	70
La Fontaine (PLU DR15)	L = 27 W = 26	2.9	470		90

Dredge (number and name)	Latitude	Longitude	Depth (m)	Site	Dredge description	Sample used in this study	Sample macroscopic description	Sample petrography
PLU DR1 Boomerang	S37°41.50 S37°40.53	E77°54.90 E77°53.91	910 760	Seamount	Mostly pillow lavas ; some with glass Volcanic brechia with sediments	PLU DR1-2-5	Fragment of vesicular pillow lavas	Phenocrysts : - Microcrysts : Ol+Pl Vesicles : ++ TAS : tholeiitic basalt
PLU DR2	S37°35.68 S37°35.67	E78°00.99 E78.00.40	1030 1010	Seamount	Only pillow lavas but different types (glassy , vesicular, aphyric and/or, sedimentary rim	PLU DR 2-1-1	Fragment of pillow lavas with fresh glass	Phenocrysts : - Microcrysts :Ol+Pl Vesicles : ++ TAS : tholeiitic basalt
PLU DR3	S37°38.90 S37°39.10	E78°09.00 E78°08.02	2025 2040	Oceanic floor	Empty			
PLU DR4	S37°51.50 S37°51.80	E78°03.50 E78°03.00	1900 1800	Oeanic floor	Only pillow lavas	PLU DR4-1-3 PLU DR4-1-5	Fragment of vesicular and aphyric pillow lavas with a small amount of glass Fragment of vesicular and	Phenocrysts : - Microcrysts : Ol+Pl Vesicles : + TAS : tholeiitic basalt Phenocrysts : - Microcrysts : Ol+Pl

Author version: J. Geophys. Res. (B: Solid Earth), vol.116(5); 2011; 17 pp; doi:10.1029/2010JB007800

							aphyric pillow lavas without glass	Vesicles : + TAS : tholeiitic basalt
	S38°00.20	E77°45.58	905		Mostly carbonate soil with lavas and glass fragment. A lot of biological organism such as coral and urchin			
PLU DR5	S38°00.21	E77°44.66	690	Seamount				
	S38°04.18	E78°13.79	1795		Blocks of fresh basalt (pillows and tubes) with a large amount of glass		Fragment of lava tube with glassy rim	Phenocrysts : - Microcrysts : Ol+Pl+Px Vesicles : + TAS : andesitic basalt
PLU DR6	S38°04.08	E78°12.23	1750	SEIR axis		PLU DR6-1-1		
	S36°19.00	E80°25.85	2000		Manganese debris			
PLU DR7	S36°19.00	E80°25.30	1860	Seamount				
	S35°39.75	E80°55.70	2000		Pillow lavas with sediments		Fragment of pillow lavas with a small amount of vesicles and Mn crust	Phenocrysts : - Microcrysts : Pl+Px Vesicles : ++ TAS : tholeiitic basalt
PLU DR8	S35°40.70	E80°55.10	1670	Seamount		PLU DR8-1-1		
PLU DR9	Dredge lost							
PLU DR10	S36°03.79	E79°43.77	1800	Inside corner	Blocks and fragments of lava with manganese crust	PLU DR10-1-1	Pillow lava with some vesicles and	Phenocrysts : Ol Microcrysts : Ol+Pl+Px Vesicles : +

							phenocrysts	TAS : tholeiitic basalt
	S36°03.69	E79°41.77	1520			PLU DR10-2-2	Pillow lava with more phenocrysts	Phenocrysts : Pl Microcrysts :Ol+Pl+Px Vesicles : - TAS : tholeiitic basalt
PLU DR11	Dredge lost							
	S32°20.91	E83°50.39	2230		Only sediments			
PLU DR12	S32°21.36	E83°49.40	2240	Seamount				
	S32°44.31	E84°04.86	1560		Diversified dredge with fragments of altered basalt, hyaloclastites, manganese, biological organism and sediments			
PLU DR13	S32°44.24	E84°04.67	1450	Seamount				
	S33°40.51	E83°04.52	2520		Fragments of lava with mangenese crust, sediments		Fragments of lava with mangenese crust	Phenocrysts : - Microcrysts : Ol+Pl+Px Vesicles : ++ TAS : tephrite
PLU DR14 Boileau	S33°40.63	E83°04.30	2440	Seamount		PLU DR14-1-1		
	S34°04.92	E83°27.41	1600		Blocks and fragments of lava, sediment	PLU DR15-1-1	Fragment of vesicular lava	Phenocrysts : - Microcrysts : Ol Vesicles : ++ TAS : tephrite
PLU DR15 La Fontaine	S34°05.64	E83°27.87	1560	Seamount		PLU DR 15-2-3	Idem with smaller	Phenocrysts : Microcrysts : Ol+Pl+Px

Author version: J. Geophys. Res. (B: Solid Earth), vol.116(5); 2011; 17 pp; doi:10.1029/2010JB007800

							vesicles	Vesicles : ++ TAS : tephrite
PLU DR16 La Bruyère	S34°03.90 S34°03.80	E82°42.70 E82°42.60	2200 2200	Seamount	Blocks and fragments of lava, sediment			
PLU DR17	S34°18.89 S34°18.22	E82°24.70 E82°25.49	2140 1980	Seamount	Fragment of altered lavas, brechia, manganese			
PLU DR18	S34°50.78 S34°51.55	E81°47.25 E81°46.34	2150 1820	Seamount	1 block of altered lava			
PLU DR19 Lamartine	S34°55.48 S34°55.21	E81°16.46 E81°16.21	1820 1440	Seamount	Numerous fragments of pillow lava and tubes. Some biological organism (coral and urchin), sediment	PLU DR19-2-2	Fragment of pillow lavas	Phenocrysts : - Microcrysts : Ol+Pl Vesicles : ++ TAS : tephrite
PLU DR20	S35°02.52 S35°03.99	E81°23.12 E81°22.28	2120 1940	Seamount	Numerous fragments of pillow lava and brechia			
PLU DR21	S39°49.08 S39°48.71	E76°51.05 E76°50.70	1400 1240	Seamount	Blocks and fragments of lava, sediment			
PLU DR22	S39°02.89 S39°02.09	E77°43.21 E77°43.25	980 860	Seamount	Blocks and fragments of lava of diverse types (vesicular, aphyric, glassy). A lot of biological organism (fish, coral, urchin, shellfish, seaspider)	PLU DR22-4-1	Fresh vesicular lava	Phenocrysts : - Microcrysts : Ol+Pl+Px Vesicles : ++ TAS : alkaline basalt
PLU DR23	S38°40.06	E77°40.45	1160	Seamount	Mostly coral and sediment,			

	S38°39.28	E77°40.48	900		two fragment of vesicular basalt			
	S37°54.99	E78°54.20	1310		Only fragment of lava, some with glass		Block with a small amount of vesicles and Mn crust	Phenocrysts : Pl Microcrysts :Pl+Pl Vesicles : + TAS : andesitic basalt
PLU DR24	S37°54.18	E78°50.70	900	Seamount		PLU DR24-1-1		
	S37°37.21	E78°37.63	1160		Mostly carbonates, fragments of altered basalt			
PLU DR25	S37°37.20	E78°36.49	900	Seamount				
	S37°30.93	E78°54.51	1710		Empty			
PLU DR26	S37°31.13	E78°54.33	1660	Seamount				
	S37°31.71	E78°55.91	1830		Three small fragments of basalt			
PLU DR27	S37°32.07	E78°55.50	1660	Seamount				
	S37°22.71	E79°16.23	1430		Fragments of massive lava, some with manganese crust, sediment and coral		Massive lava with a lot of small vesicles	Phenocrysts : Ol+Pl Microcrysts : Pl Vesicles : + TAS : tholeiitic basalt
PLU DR28	S37°23.19	E79°15.78	1350	Seamount		PLU DR28-1-1		
	S36°10.28	E80°34.37	2050		Fragments of lava			
PLU DR29	S36°10.42	E80°34.08	1810	Seamount				
	S35°09.47	E80°41.37	1100		Blocks and fragments of lava of diverse types (vesicular and/or aphyric). A lot of biological organism (fish,		Fragment of aphyric and vesicular lavas	Phenocrysts : - Microcrysts : Ol+Pl Vesicles : ++ TAS : tephrite
PLU DR30 Apollinaire	S39°09.95	E80°41.37	820	Seamount		PLU DR 30-1-1		

					coral, urchin, shellfish)			
	S34°22.67	E81°30.25	2300		Hyalocalstites with altered			
PLU DR31	S34°22.84	E81°30.74	1920	Seamount	basalt			
PLU DR32	S34°34.98	E81°56.52	1140		Block of lavas			
Sand	S34°35.12	E81°56.66	1140	Seamount				
	S36°18.20	E81°17.05	3990	fracture	Mostly sediments with some			
PLU DR33	S36°18.19	E81°16.33	3600	zone	manganese nodule			
	S37°24.74	E80°03.84	3050		Fragments of pillow lavas,		Fragment of	Phenocrysts : Ol+Pl
					sediments		pillow lava	Microcrysts : Ol+Pl
				Oceanic			with some	Vesicles : +
PLU DR34	S37°24.75	E80°03.54	2850	floor		PLU 34-1-1	vesicles	TAS : tholeiitic basalt
PLU DR35	S38°10.65	E79°12.50	1100		Fragments of pillow lavas,			
Verlaine	S38°10.80	E79°11.70	860	Seamount	sediments and coral			
	S38°02.16	E79°38.82	3000	fracture	Only sediment			
PLU DR36	S38°02.24	E79°39.04	2400	zone				
	S38°22.72	E77°41.20	1080		Fragment of lavas, red			
					sediment, biological organism			
PLU DR37	S38°21.84	E77°39.85	960	Seamount	(coral, starfish, shellfish)			
	S38°17.34	E77°46.64	1200		Only sediment and biological			
PLU DR38	S38°18.97	E77°46.76	1000	Seamount	organism (coral, shellfish)			
	S36°44.19	E78°55.23	1470		Large amount of pillow lavas		Fragment of	Phenocrysts : -
PLU DR39							aphyric	Microcrysts : Ol+Pl
Rimbaud	S36°44.09	E78°55.03	960	Seamount		PLU DR39-1-1	pillow lava.	Vesicles :+

							Fresh aspect but a small Mn crust	TAS : tholeiitic basalt
PLU DR40	S36°23.75 S36°23.17	E79°16.46 E79°15.87	1520 1260	Seamount	Only sediment with fragment of manganese			

Author version: J. Geophys. Res. (B: Solid Earth), vol.116(5); 2011; 17 pp; doi:10.1029/2010JB007800

Sample Ar Exp.n°	Whole rock K_2O (wt%)	Whole rock Nb (ppm)	LOI (%)	K* (wt.%)	Weight molten (g)	$^{40}Ar^*$ (%)	$^{40}Ar^*$ (10^{-12} moles/g) ±1σ	$^{40}Ar^*$ (10^{-12} moles/g) weighted mean ±1σ	Age mean value Ma (±2σ)
DR 14-1-1	*1.76*	*57.6*	*3.44*						
7833				*0.664 ± 0.007*	*0.92175*	*36.300*	*9.937 ± 0.051*		
7847				"	*0.98453*	*28.741*	*9.419 ± 0.048*	*9.664 ± 0.035*	*8.37 ± 0.18*
DR 24-1-1	0 .19	4.78	0.29						
7856				0.149 ± 0.002	1.05633	17.618	1.431 ± 0.014		
7880				"	0.71068	16.488	1.449 ± 0.015	1.439 ± 0.010	5.56 ± 0.14
DR 8-1-1	0.39	17.6	0.97						
7780				0.183 ± 0.002	0.59650	8.685	1.429 ± 0.024		
7797				"	1.77616	13.496	1.406 ± 0.009	1.409 ± 0.008	4.43 ± 0.10
DR 10-2-2	0.37	9.80	0.28						
7782				0.183 ± 0.002	0.72771	10.671	1.174 ± 0.019		
7799				"	1.72055	10.992	1.163 ± 0.009	1.165 ± 0.008	3.67 ± 0.09
DR 10-1-1	0.42	8.27	0.25						
7885				0.291 ± 0.003	1.24193	7.075	1.533 ± 0.014		
7901				"	0.94859	6.791	1.525 ± 0.015	1.529 ± 0.010	3.03 ± 0.07
DR 34-1-1	0.81	24.7	0.56						
7675				0.631 ± 0.006	1.16145	8.848	2.920 ± 0.020		
7691				"	1.00776	9.702	2.870 ± 0.019	2.894 ± 0.014	2.64 ± 0.06
DR 15-2-3	*1.81*	*70.7*	*0.69*						
7687				*1.619 ± 0.016*	*0.49595*	*15.835*	*5.909 ± 0.034*		
7703				"	*0.43202*	*17.846*	*5.754 ± 0.033*	*5.831 ± 0.023*	*2.08 ± 0.04*
DR 28-1-1	0.12	2.64	0.02						
7717				0.075 ± 0.001	1.64586	2.977	0.248 ± 0.008		
7732				"	1.71827	2.841	0.240 ± 0.007	0.244 ± 0.005	1.87 ± 0.09
DR 19-2-2	*1.90*	*62.2*	*1.11*						
7669				*1.602 ± 0.016*	*1.22852*	*9.361*	*2.886 ± 0.017*		
7685				"	*1.01565*	*8.556*	*2.911 ± 0.019*	*2.898 ± 0.013*	*1.04 ± 0.02*

Sample Ar Exp. n°	Whole rock K_2O (wt%)	Whole rock Nb (ppm)	LOI (%)	K* (wt.%)	Weight molten (g)	$^{40}Ar^*$ (%)	$^{40}Ar^*$ (10^{-14} moles/g) ±1σ	$^{40}Ar^*$ (10^{-14} moles/g) weighted mean ±1σ	Age mean value ka (±2σ)
DR 15-1-1	*2.05*	*79.2*	*0.41*						
7884				*1.752 ± 0.018*	*1.04925*	*5.310*	*207.78 ± 1.92*		
7900				*"*	*" 0.73490*	*4.470*	*208.97 ± 2.00*	*208.35 ± 1.387*	*686 ± 15*
DR 39-1-1	0.20	4.3	-0.32						
7834				0.166 ± 0.002	0.95800	1.709	15.890 ± 1.00		
7857				"	" 1.00300	1.416	15.611 ± 1.56	15.810 ± 0.837	549 ± 59
DR 2-1-1	0.54	14.3	-0.35						
7855				0.440 ± 0.004	1.05633	0.857	24.853 ± 1.16		
7891				"	" 1.00686	0.978	21.041 ± 1.39	23.290 ± 0.893	305 ± 24
DR 4-1-3	0.67	29.0	-0.36						
7865				0.548 ± 0.006	1.16565	0.245	10.098 ± 1.46		
7881				"	" 1.20200	0.227	13.761 ± 1.16	12.681 ± 0.909	133 ± 19
DR 30-1-1	*2.09*	*74.1*	*-0.32*						
7781				*1.694 ± 0.017*	*0.77183*	*1.612*	*18.974 ± 1.44*		
7809				*"*	*" 0.46385*	*0.330*	*17.363 ± 2.62*	*18.6018 ± 1.262*	63 ± 9
DR 1-2-4	0.59	28.9	-0.40						
7670				0.515 ± 0.005	1.02667	-0.041	-		
7702				"	" 1.46920	-0.025	-	-	-
DR 22-4-1	0.55	19.7	1.027						
7672				0.457 ± 0.005	1.11685	-0.018	-		
7704				"	" 1.13631	-0.017	-	-	-
DR 6-1-1	1.33	46.4	0.61						
7673				0.996 ± 0.010	0.93340	0.237	2.126		
7716				"	" 1.01350	-0.256	-	-	-
DR 4-1-5	0.62	24.8	-0.32						
7674				0.573 ± 0.006	1.01481	-0.177	-		
7690				"	" 1.01820	-0.060	-	-	-